J Mol Model (2013) 19:5317–5325
DOI 10.1007/s00894-013-2024-4

ORIGINAL PAPER

Structure-property relationships for three indoline dyes used in dye-sensitized solar cells: TDDFT study of visible absorption and photoinduced charge-transfer processes

Huixing Li · Maodu Chen

Received: 11 July 2013 / Accepted: 26 September 2013 / Published online: 24 October 2013

Abstract The electronic structures of three D-A-π-A indoline dyes (WS-2, WS-6, and WS-11) used in dye-sensitized solar cells (DSSCs) were studied by performing quantum chemistry calculations. The coplanarity of the A-π-A segment and distinct noncoplanarity of the indoline donor part of each dye were confirmed by checking the calculated geometric parameters. The relationships between molecular modifications and the optical properties of the dyes were derived in terms of the partial density of states, absorption spectrum, frontier molecular orbital, and excited-state charge transfer. 3D real-space analysis of the transition density (TD) and charge difference density (CDD) was also performed to further investigate the excited-state features of the molecular systems, as they provide visualized physical pictures of the charge separation and transfer. It was found that modifying the alkyl chain of the bridge unit near the acceptor unit is an efficient way to decrease dye aggregation and improve DSSC efficiency. Inserting a hexylthiophene group next to the donor unit leads to a complicated molecular structure and a decrease in the charge-transfer ability of the system, which has an unfavorable impact on DSSC performance.

Keywords Dye-sensitized solar cell · Organic sensitizer · TDDFT · Absorption spectrum · Charge transfer · Charge difference density

H. Li · M. Chen (✉)
School of Physics and Optoelectronic Technology, and College of Advanced Science and Technology, Dalian University of Technology, Dalian 116024, People's Republic of China
e-mail: mdchen@dlut.edu.cn

Introduction

The dye sensitizer plays a vital role in a dye-sensitized solar cell (DSSC), as it is responsible for harvesting the light and injecting electrons into the conduction band of the semiconductor surface [1–12]. The most promising photosensitizers are ruthenium (Ru) complexes (such as N3, N719, and black dyes), which show stable photoelectric conversion efficiencies of about 11% [9, 13, 14]. And a DSSC based on a zinc (Zn) porphyrin sensitizer is reported to have an efficiency of >12% [15]. However, metal-free organic dye sensitizers have also attracted interest due to their low cost, high molar extinction coefficients, ready availability, environmentally friendly features, and flexibility in terms of molecular design. One typical family of pure organic sensitizers that contain electron-donating and electron-accepting units that are linked by a π-conjugated bridge is commonly known as the D-π-A dyes [2, 16–21]. The donor unit in such a dye is usually an electron-rich group that injects electrons into the TiO_2 semiconductor surface after the dye has been excited through the absorption of light. The acceptor unit (anchoring group) is usually a strongly electron-withdrawing group that accepts electrons from the donor part and couples with the TiO_2 surface. The π-bridge unit facilitates electron transfer and broadens the absorption spectrum. By modifying the structure of the π-conjugated bridge and varying the substituents on the donor and acceptor units, it is possible to adjust the highest occupied molecular orbital (HOMO) and the lowest unoccupied molecular orbital (LUMO) of the sensitizer in order to enhance the electronic coupling between the dye molecule and the TiO_2 surface [19, 21–24], thus improving the power-to-current conversion efficiency of the DSSC.

However, the highest conversion efficiency that has been attained by a metal-free D-π-A organic-sensitizer-based DSSC

is still below that afforded by ruthenium-complex-based ones. To obtain a highly efficient DSSC based on a D-π-A organic dye, one of the challenging problems that must be solved is that the aggregation of dye on the surface of the TiO_2 film must be suppressed, as significant surface aggregation leads to unfavorable back-transfer of electrons and decreases the open-circuit voltage (V_{oc}), ultimately reducing the overall efficiency of the DSSC [25, 26]. In order to resolve this problem, additives such as deoxycholic acid (DCA), 4-*tert*-butylpyridine (TBP), and chenodeoxycholic acid (CDCA) have been added to DSSC devices [27–30]. However, while these additives do dissociate the π-stacked dye aggregates, they also reduce the amount of organic dye that is loaded onto the TiO_2 surface [30].

Other creative solutions to this problem are to incorporate subordinate electron-withdrawing groups into the π-bridge unit to act as an auxiliary acceptor, thus tailoring the molecular configuration and optimizing orbital levels, or to introduce alkyl chains that suppress dye aggregation. Naturally, the concept of a specific donor-acceptor-π bridge-acceptor (D-A-π-A) configuration has been proposed [31], emphasizing the electron-withdrawing effect of an auxiliary acceptor but not a simple extension of the π-bridge building block in a traditional D-π-A dye. Recently, Zhu and coworkers synthesized a series of novel D-A-π-A metal-free sensitizers (WS-1 to WS-4) by inserting a strongly electron-withdrawing unit, the benzothiadiazole (BTD) group, into the conjugated bridge of a traditional D-π-A dye molecule [32]. The combined BTD unit shows several advantages, such as broadening the range of absorption wavelengths in the ultraviolet–visible spectrum and increasing photostability [32–35]. More recently, Wang and coworkers designed and synthesized two D-A-π-A organic dyes, WS-6 and WS-11, based on the WS-2 sensitizer, by introducing an alkyl chain into the thiophene bridge and inserting a hexylthiophene unit between the donor and BTD units [33]. They experimentally investigated and compared the photophysical and electrochemical properties and the corresponding photovoltaic device performances of the three sensitizers (WS-2, WS-6, and WS-11). The influence of the incorporated alkyl chain and hexylthiophene on the conversion efficiency of the sensitized solar cell was further demonstrated.

In the work described in the present paper, in order to determine how the introduced alkyl chain and the additional hexylthiophene substituent impact the optical characteristics of the dyes and the performance of the solar cell device, the ground-state geometries and the excited-state properties of three D-A-π-A sensitizers (WS-2, WS-6, and WS-11) were studied by performing quantum chemistry calculations. We focused in particular on the mechanism of the charge-transfer process, since it is one of the most important steps in the photon-to-electricity conversion process performed by a DSSC.

Methods

The structures of WS-2, WS-6, and WS-11 were constructed manually according to [32, 33]. Ground-state geometries were fully optimized using density functional theory (DFT) [36] with the long-range-corrected CAM-B3LYP [37] and B3LYP [38–40] hybrid functionals and the 6-311g basis set [41–46]. No imaginary frequencies were present in the frequency analysis of the optimized structures. The first hyperpolarizabilities in a static field were calculated at the same levels of theory. The finite field (FF) approach was employed, since it is generally suitable for complex systems and computationally inexpensive [47, 48]. The response of a molecule in a static electronic field (F) can be expressed via [49–51]

$$E(F) = E_0 - \mu_i F_i - \frac{1}{2}\alpha_{ij} F_i F_j - \frac{1}{6}\beta_{ijk} F_i F_j F_k - \cdots\cdots, \quad (1)$$

where E_0 is the unperturbed energy of the molecules, F_i is the field at the origin, and μ_i, α_{ij}, and β_{ijk} are the dipole moment, polarizability, and the static first hyperpolarizability, respectively. The components of β can be calculated using the following equation:

$$\beta_i = \beta_{iii} + \frac{1}{3}\sum_{i \neq j}\left(\beta_{ijj} + \beta_{jij} + \beta_{jji}\right). \quad (2)$$

Here, i and j represent the x, y, and z components of β, respectively. The magnitude of the total static first hyperpolarizability can be expressed as

$$\beta_{tot} = \left(\beta_x^2 + \beta_y^2 + \beta_z^2\right)^{1/2}. \quad (3)$$

According to Kleinman symmetry [52], the complete expression for the total static first hyperpolarizability is

$$\beta_{tot} = \left[\left(\beta_{xxx} + \beta_{xyy} + \beta_{xzz}\right)^2 + \left(\beta_{yyy} + \beta_{yzz} + \beta_{yxx}\right)^2 + \left(\beta_{zzz} + \beta_{zxx} + \beta_{zyy}\right)^2\right]^{1/2.} \quad (4)$$

The vertical excitation energies for the ground-state equilibrium geometries were determined using time-dependent DFT (TDDFT) [53]. To better study the charge-transfer properties of the three dyes, the CAM-B3LYP functional was employed with the highly accurate basis set 6-311g(d,p) in the excited-state calculations. To verify the theoretical results using experimental data, all DFT/TDDFT calculations were combined with the integral equation formalism version of the

polarizable continuum model (IEF-PCM) [54–57], and dichloromethane was the solution employed in calculations according to the experimental setting [33]. The partial density of states (PDOS) was visualized with GaussSum software [58]. The transition density (TD) and charge difference density (CDD) were obtained through visualized three-dimensional (3D) real-space analysis [59–61]. All calculations were performed within the quantum-chemical software package Gaussian 09 [62].

Results and discussion

Two-dimensional sketches and the optimized geometries of WS-2, WS-6, and WS-11 in dichloromethane solvent are depicted in Figs. 1 and 2, respectively. WS-2 is a typical D-A-π-A organic dye molecule containing an indoline derivative (donor), a BTD group (auxiliary acceptor), a thiophene ring (π-bridge), and cyanoacrylic acid (acceptor). Notably, the electron-deficient BTD unit functions as an electron-trapping unit rather than merely an extension of the π-conjugated bridge. The A-π-A system of the calculated geometry of WS-2 is clearly coplanar, which may enhance intramolecular electron transport to the acceptor and facilitate bathochromic shifts of the absorption peaks in the ultraviolet–visible spectrum. Compared with WS-2, the WS-6 molecule has an extra alkyl chain on the thiophene bridge, which efficaciously restrains dye–dye interactions relative to WS-2 [33]. Also, the coplanarity along the A-π-A section of WS-6 ensures a wide absorption response region and good electron-transfer ability,

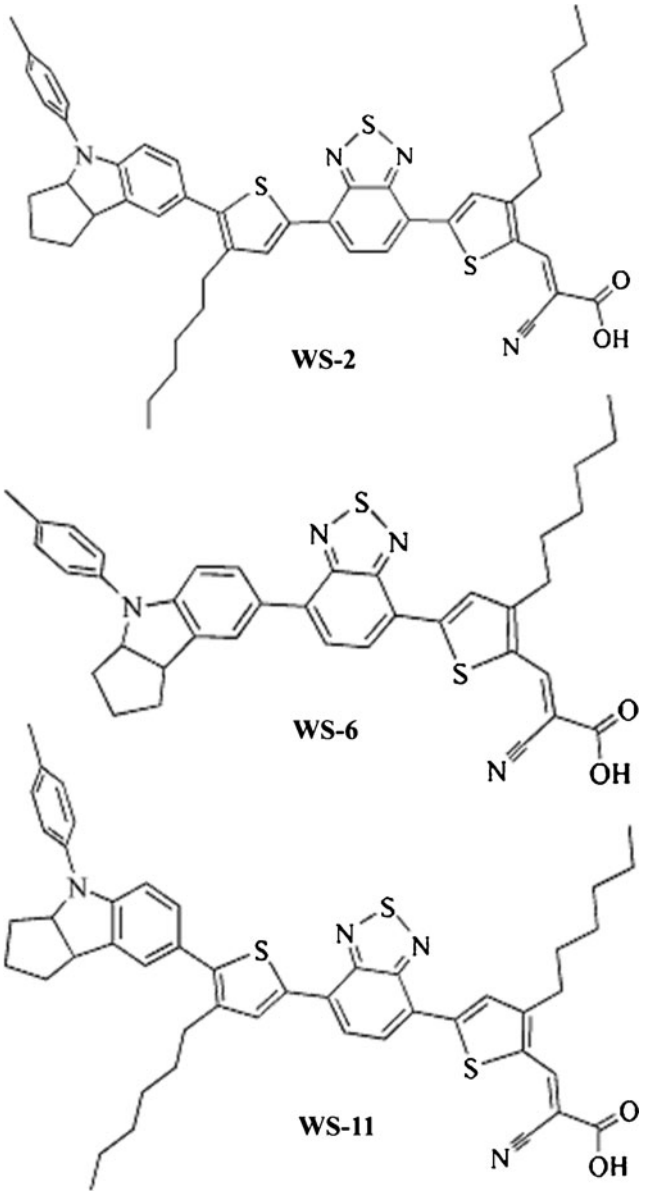

Fig. 1 2D sketches of the three dyes WS-2, WS-6, and WS-11

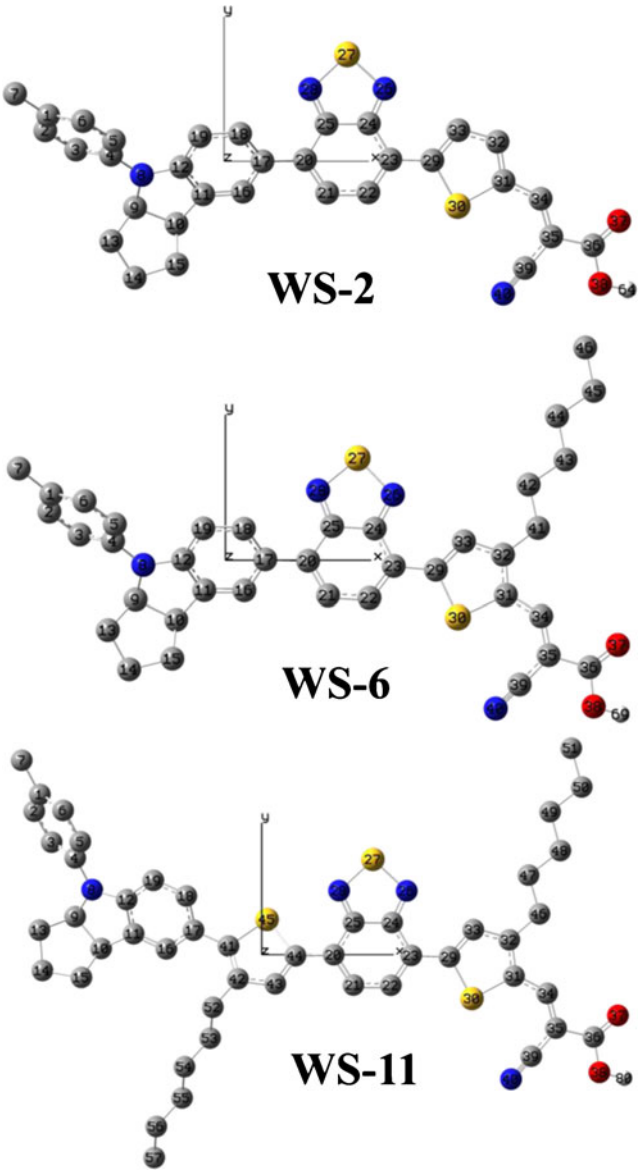

Fig. 2 Optimized structures of the three dyes WS-2, WS-6, and WS-11

Table 1 Calculated structural parameters, including crucial bond lengths (in Å) and dihedral angles (in degrees) for the three dyes, as calculated with the B3LYP and CAM-B3LYP functionals

	CAM-B3LYP			B3LYP		
	WS-2	WS-6	WS-11	WS-2	WS-6	WS-11
C3–C4	1.3994	1.3986	1.3999	1.4058	1.4055	1.4071
C4–C8	1.4100	1.4102	1.4086	1.4178	1.4177	1.4155
C8–C9	1.4856	1.4858	1.4854	1.4965	1.4972	1.4958
C8–C12	1.3909	1.3908	1.3945	1.3895	1.3895	1.3949
C17–C20	1.4720	1.472	–	1.4666	1.4668	–
C17–C41	–	–	1.4656	–	–	1.4595
C20–C21	1.3698	1.3698	1.3717	1.3893	1.3896	1.393
C23–C29	1.4532	1.4533	1.4529	1.4452	1.4454	1.4444
C31–C34	1.4200	1.4148	1.4156	1.4119	1.4075	1.408
C34–C35	1.3591	1.3629	1.3622	1.3762	1.3801	1.3796
D(5,4,8,12)	−39.0	−40.0	−38.8	−40.4	−41.1	−39.4
D(18,17,20,21)	145.7	145.7	–	151.1	152.5	–
D(18,17,41,42)	–	–	134.7	–	–	141.6
D(21,20,44,45)	–	–	−160.1	–	–	−173.4
D(24,23,29,30)	−180.0	179.3	179.6	−178.7	−178.9	−179.7

like WS-2. For WS-11, the additional hexylthiophene is inserted between the indoline donor and BTD unit present in the WS-6 molecule, which leads to a bent D-A-π-A structure. The relationships between these structural modifications and the absorption, orbital energy level, and excited-state charge transfer characteristics of these molecules will be further discussed and clarified in subsequent paragraphs.

Table 1 gives the geometric parameters of the three dyes, including crucial bond lengths and dihedral angles, as calculated using the CAM-B3LYP and B3LYP functionals with the 6-311g basis set. The listed bond lengths of the three dyes calculated using the two functionals are similar. The two functionals also give similar results for the dihedral angles between the BTD and thiophene units of the three dyes: the dihedral angle *D*(24,23,29,30) is −180.0° for WS-2, 179.3° for WS-6, and 179.6° for WS-11 with CAM-B3LYP, and −178.7°, −178.9°, and −179.7° (respectively) with B3LYP, all of which indicate that the A-π-A segment is coplanar. However, the functionals yield significantly different results for the dihedral angle between the indoline donor and BTD units of WS-2 and WS-6 and for the dihedral angle between the hexylthiophene and BTD units of WS-11. The dihedral angle *D*(18,17,20,21) between the indoline donor and BTD units is 145.7° for WS-2 and 145.7° for WS-6 with CAM-B3LYP, while these angles are notably larger with B3LYP: 151.1° and 152.5°, respectively. The dihedral angles *D*(18,17,41,42) and *D*(21,20,44,45) for WS-11 are 134.7° and −160.1° with CAM-B3LYP but 141.6° and −173.4° with B3LYP, respectively. The significant differences in the results obtained using the two functionals for the above dihedral angles probably arise due to the presence of strong steric hindrance effects in these systems [63, 64]. There are strongly repulsive interactions between the indoline donor unit and the BTD unit in WS-2 and WS-6, and between the hexylthiophene unit and the BTD unit in WS-11. Another possible reason may be the high proportion of Hartree–Fock (HF) exchange for the long-range part of CAM-B3LYP, since this plays a crucial role in ground-state geometry optimization, so accounting for this leads to more accurate ground-state structures [37, 65, 66].

We also checked the static first hyperpolarizability of each D-A-π-A dye, due to its influence on the nonlinear optical (NLO) properties of the π-conjugated organic molecules. All of the calculations of the first hyperpolarizability components were carried out using the long-range-corrected functional CAM-B3LYP and the 6-311g(d,p) basis set, which has been demonstrated to greatly reduce overestimation of the polarization characteristics of π-conjugated materials [66, 67]. The calculated first hyperpolarizability components are listed in Table 2, and these were used to ascertain the effect of structural modification on the polarization of each molecular system and to better understand the ground-state structures. The calculated results show the following trend in total static first hyperpolarizability for the three dyes: WS-6<WS-2<WS-11. From Table 2, the dominant component (along the *x*-axis) of the static first hyperpolarizability is consistent with the direction of charge transfer along the donor-π bridge-accepter molecular skeleton. The total static first hyperpolarizabilities of WS-2 and WS-6 are quite similar to each other, indicating that the addition of the alkyl chain in WS-6 has a relatively minor impact on its NLO properties. The total static first hyperpolarizability of WS-11 is much larger than those of the other two. There are two possible reasons for this: one is the longer conjugated length of the whole molecular skeleton, and the other is the increased complexity of the structure of WS-11 after inserting hexylthiophene between the indoline donor and BTD units. NLO activity is generally a reflection of the degree of the delocalization of π electrons from donor to acceptor, but WS-11, which has the largest hyperpolarizability of the three dyes, results in the least efficient

Table 2 Static first hyperpolarizabilities of WS-2, WS-6, and WS-11 (in a.u.), as calculated at the CAM-B3LYP/6-311g(d,p) level of theory

	β_{xxx}	β_{xxy}	β_{xyy}	β_{yyy}	β_{xxz}	β_{yyz}	β_{xzz}	β_{yzz}	β_{zzz}	β_{total}
WS-2	87943	−7937	2142	−614	−2666	52	−403	20	59	90123
WS-6	86498	−12574	2734	−1128	2474	333	−304	5	−31	90019
WS-11	92095	−18185	3483	−466	−70	280	−226	11	−56	97157

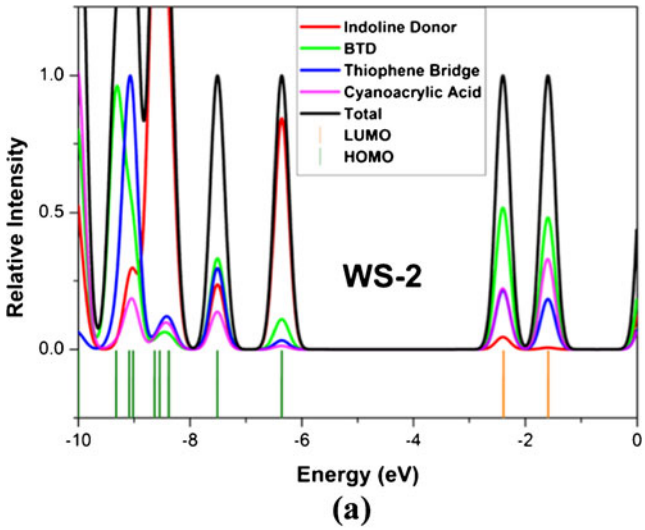

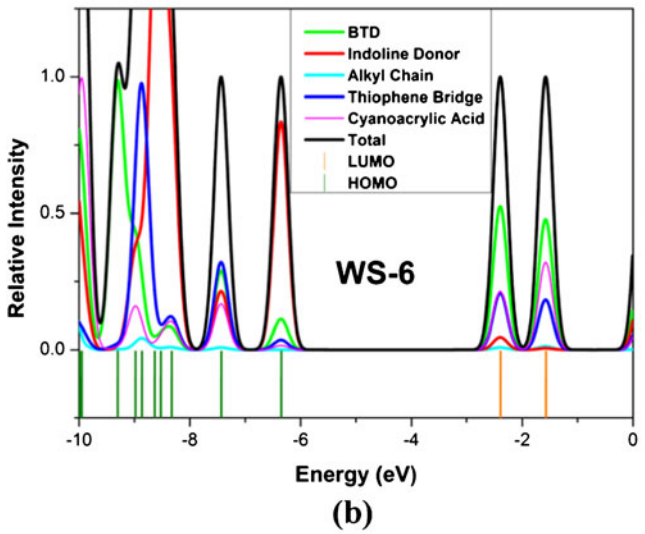

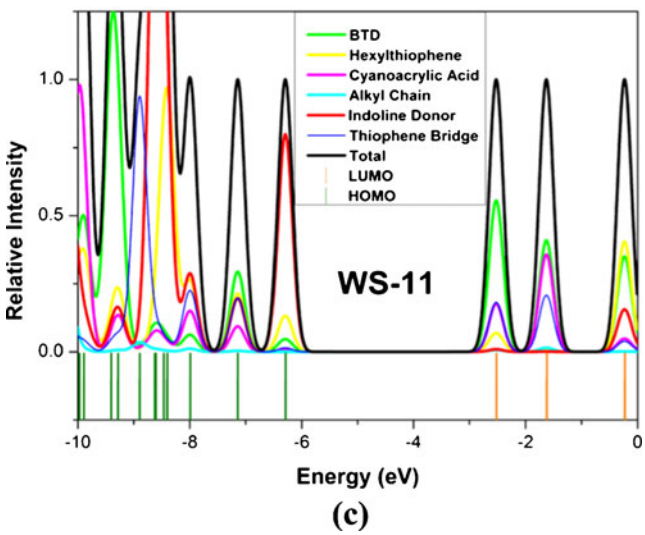

Fig. 3a–c Partial density of states (PDOS) projected onto different atomic species for the molecules WS-2 (**a**), WS-6 (**b**), and WS-11 (**c**)

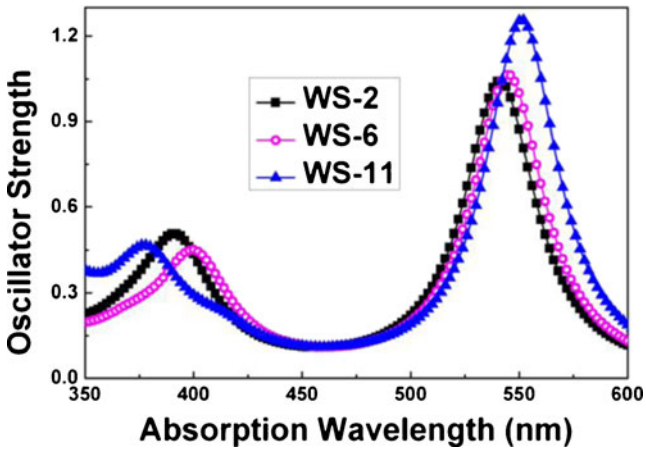

Fig. 4 Calculated absorption spectra of the three dyes (WS-2, WS-6, and WS-11) in dichloromethane

DSSC. This may be due to the noncoplanarity of the π-conjugated moieties along the A-π-A section of the molecule. Therefore, the complicated noncoplanarity of the π-conjugated bridge may have an unfavorable effect on electron transfer and injection, so this structural motif should be avoided when designing the sensitizers used in DSSC devices.

The partial density of states (PDOS) in Fig. 3 can help us to further understand the ground-state geometries of the sensitizers by indicating the percentage contribution of each atomic species to each molecular orbital. Generally, except for the alkyl chains, all of the species contribute to the total density of states for the HOMOs and LUMOs. Across the whole energy range, the density of states from the alkyl chains (cyan line) in WS-6 and WS-11 can hardly be seen, indicating that the alkyl chains are not involved in the intramolecular charge-transfer process and exclusively suppress dye aggregation. The alkyl chain is not an active unit of the molecule during excitation by light. In addition, the HOMOs are found to locate broadly across the whole molecular skeleton, albeit mainly on the indoline donor group. Delocalization of the HOMOs promotes intermolecular hole-hopping and carrier mobility, ensuring good photochemical activity of the dyes. The electronic density of the LUMOs for the three dyes is essentially spread across the thiophene bridge and cyanoacrylic acid unit, enhancing electron-cloud overlap between the anchoring group (acceptor unit) and the semiconductor film surface, and promoting barrierless electron transfer from the LUMO of the sensitizer to the TiO_2 conduction band. According to Fig. 3, the HOMO levels of the dyes are very similar, whereas the LUMO level of WS-11 (−2.52 eV) is more negative than the LUMO levels of the other two dyes (−2.39 eV for both WS-2 and WS-6), which is indicative of a stronger thermodynamic driving force for electron injection into the TiO_2 surface [68, 69]. Accordingly, the HOMO–LUMO energy gap of WS-11 is the smallest among the three dyes, leading to the strongest and broadest absorption, as also noted experimentally [33]. In

Table 3 The calculated vertical excitation energy E (in eV and nm), oscillator strength f, main configuration interaction (CI) expansion coefficient, and the corresponding percentage contribution (more than 30%) to each excited state for each of WS-2, WS-6, and WS-11 in dichloromethane. Only the characteristic parameters of strong excited states (those with oscillator strengths of >0.3) are listed

	CAM-B3LYP				B3LYP		Expt. [33]
	Excited state	E (eV, nm)	CI	f	E (eV, nm)	f	E (eV, nm)
WS-2	S_1	2.29 (541)	H →L 0.62021 (77%)	1.0292	1.53 (810)	0.8808	2.27 (546)
	S_2	3.16 (392)	H-1 →L 0.51672 (53%)	0.4228			
	S_7	4.25 (292)	H →L+2 0.37895 (29%)	0.3738			
WS-6	S_1	2.28 (545)	H →L 0.62081 (77%)	1.0517	1.53 (809)	0.8990	2.27 (547)
	S_2	3.10 (400)	H-1 →L 0.52497(55%)	0.3767			
	S_7	4.23 (293)	H →L+2 0.35243 (25%)	0.3759			
WS-11	S_1	2.25 (551)	H →L 0.51920 (54%) H-1 →L 0.44099 (39%)	1.2427	1.32 (940)	0.8568	2.23 (557)
	S_3	3.28 (378)	H-1 →L+1 0.50049 (50%)	0.3331			
	S_7	3.97 (313)	H →L+2 0.50789 (52%)	0.7401			

Fig. 3c, the PDOS from the additional hexylthiophene group of WS-11 presents an extensive distribution of occupied molecular orbitals across the full energy range, and a comparable contribution to HOMO-2 to that of the indoline donor group. We can assume that the additional hexylthiophene unit exerts some influence on the charge separation and transport in the sensitizer. Comparing the PDOSs of WS-2 and WS-6 to that of WS-11 in Fig. 3, it is clear that incorporating the hexylthiophene unit between the indoline donor and the BTD unit reduces the contributions of the bridge to the HOMO and HOMO-1. Hence, aside from attracting the electron from the donor part, the additional hexylthiophene unit may simultaneously block or delay charge transport to the BDT and thiophene units. Later, this preliminary study and exploration of the effect of structural modification on the optical properties of the dyes using the PDOS method will be validated and complemented by the results of visualized frontier molecular orbital and excited-state charge-transfer analysis.

Figure 4 shows the absorption spectra of the three D-A-π-A dyes, which were simulated by Lorentzian functions with a full width at half-maximum (FWHM) of 20 nm. The corresponding transition features for relatively strong (f>0.3) excited states are listed in Table 3, including the vertical excitation energy E (in nm and eV), the oscillator strength f, and the main configuration interaction (CI) coefficient along with the percentage contribution (more than 30%) to each excited state. The frontier molecular orbitals involved in the transitions are given in Fig. 5. From Table 3, the TD-B3LYP-calculated absorption features for the three dyes are strongly redshifted compared with the experimental results and the TD-CAM-B3LYP-calculated results. The same trend has also been observed in many studies of the optical properties of sensitizers in DSSCs, especially large conjugated organic dyes with strong charge-transfer characteristics [70]. This deviation, which is caused by the underestimation of the transition energy when applying traditional hybrid B3LYP, can be ameliorated by using the range-separated hybrid functional CAM-B3LYP, which increases the fraction of exact Hartree–Fock exchange as the interelectronic distance increases [70]. According to Fig. 4, there are two strong absorption peaks in the UV-visible spectrum, and these are in good agreement with the experimentally observed peak positions and relative intensities. The center wavelengths of the absorption peaks for the three dyes are 541 nm for WS-2, 545 nm for WS-6, and 551 nm for WS-11, respectively, suggesting that they have nearly the same absorption response regions. The calculated results agree quite well with the experimental data (546 nm for WS-2, 547 nm for WS-6, and 557 nm for WS-11) [33] and previous theoretical reports [71–73]. In particular, the oscillator strength of WS-11 (f=1.2427) is significantly larger than those of WS-2 (f=1.0292) and WS-6 (f=1.0517), which implies that it has the strongest absorption intensity. However, the photoelectric conversion efficiency for the WS-11-based DSSC is also much lower than those for WS-2 and WS-6 [33]. From Table 3, for all three dyes, the strongest absorption band comes from the first excited state (S_1), corresponding to the

HOMO–LUMO transition. Looking at the frontier molecular orbitals in Fig. 5, the HOMO is mainly located on the indoline donor part, while the LUMO is mainly localized on the thiophene bridge and the cyanoacrylic acid acceptor. Hence, S_1 is an intramolecular charge-transfer excited state (ICT) where electron transfer occurs from the indoline donor to the cyanoacrylic acid acceptor. The incorporation of the alkyl chain into the thiophene group takes up a great deal of space and increases the noncoplanar character of the whole complicated molecular system, which may reduce the aggregation of dye on the semiconductor surface. It is known that an organic sensitizer with lots of delocalized electrons on its conjugated bridges (e.g., the thiophene unit) will readily participate in intermolecular π–π stacking interactions with an adjacent molecule [74, 75]. Figure 5 also shows that no frontier molecular orbital is localized on the alkyl chain, which indicates that it functions as a spacer that shifts the LUMO orbital (which is occupied when the dye is in the excited state) away spatially and thus decreases dye–dye interactions [76]. This may also account for the high efficiency of WS-6, and it is consistent with the previous PDOS analysis and experimental results. Another relatively strong excited state, S_2 (f=0.4228), for WS-2 represents the π–π* transition from HOMO-1 to LUMO, and is the secondary absorption band in the absorption spectrum. For WS-6, another two strong excited states, S_2 and S_7, are seen aside from S_1; these involve higher-level molecular orbitals. The main transitions associated with S_2 and S_7 are the HOMO-1 → LUMO and HOMO → LUMO+2 transitions, respectively. These are π–π* transitions (see Fig. 5b). In summary, compared with WS-2, WS-6 possesses a similar first static hyperpolarizability and similar distributions of active molecular orbitals on the main body of the molecule, except for the alkyl side chain, indicating that they have comparable photochemical activities. The high efficiency of the WS-6-based solar cell is derived from the spatial inhibition of dye aggregation caused by the insertion of the alkyl chain.

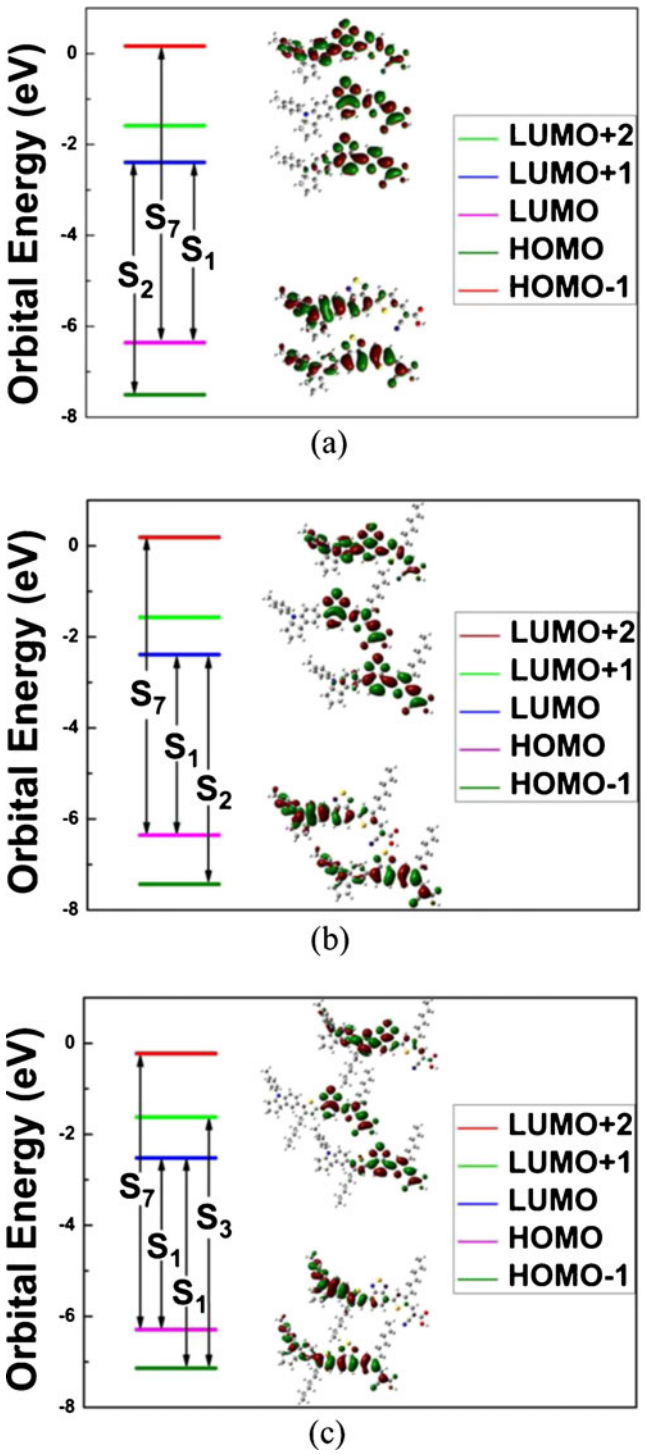

Fig. 5a–c The frontier molecular orbitals and the orbital energy levels for **a** WS-2, **b** WS-6, and **c** WS-11

Table 4 The transition density (TD) and charge difference density (CDD) for the first excited state of WS-2, WS-6, and WS-11. *Green* and *red* colors represent hole and electron densities, respectively

	TD	CDD
WS-2	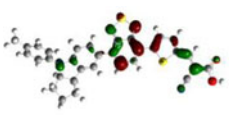	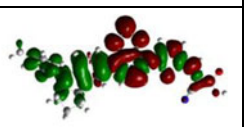
WS-6	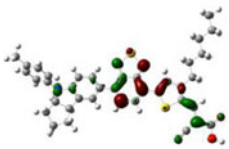	
WS-11	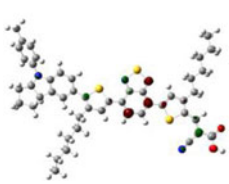	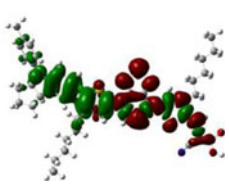

Unlike in WS-2 and WS-6, two main transitions are associated with the S_1 excited state of WS-11. One corresponds to the HOMO →LUMO ICT process, with a percentage contribution of only 54%, which is much smaller than those seen for WS-2 and WS-6 (both are 77%). The other is the π–π* transition from HOMO-1 to the LUMO localized on the bridge and acceptor, which makes a considerable percentage contribution (39%) to the S_1 excited state, and may be unfavorable to electron transfer from the donor part to the acceptor and then to the conduction band on the TiO_2 electrode surface. This may be an important reason for the low efficiency of the WS-11-based DSSC. In addition, the PDOS spectrum of WS-11 in Fig. 3c shows that the HOMO electronic density is low on the thiophene bridge and cyanoacrylic acid acceptor and even on the BTD unit, which may lead to a decrease in the electron delocalization and stability of this molecular system. Besides, inserting the hexylthiophene group results in a longer distance over which electrons must be transported, which could result in a decrease in the number of validly injected electrons.

To further investigate the microscopic charge-transfer processes of the three dyes, 3D real-space analysis of the TD (transition density) and CDD (charge difference density) was performed. This technique has been widely applied to organic molecular systems [59–61, 77, 78]. The TD and CDD indicate the region where charge separation occurs and the charge redistribution changes after excitation. More details can be found in [79–81]. A comparison of the TD and CDD populations of WS-2, WS-6, and WS-11 is provided in Table 4, where only the first excited states with the strongest intensities are included. According to the CDDs, the hole density and electron density for the S_1 excited state of each dye are concentrated mainly on the donor unit and the acceptor unit, respectively. The charge-transfer distance for WS-11 is clearly longer than those for the other two. No great differences in the TDs of WS-2 and WS-6 were observed. They were all generally spread across the whole molecular system, indicating that these two dyes have comparably strong charge-transfer abilities. Besides, the electronic density on the alkyl chain of WS-6 is low, indicating that this chain barely affects electron injection into the TiO_2 surface. However, the TD coverage for WS-11 is much smaller than those for WS-2 and WS-6, implying a weaker intramolecular transition dipole moment. This is unfavorable for distant intramolecular electron transfer across the molecular skeleton, and could be another reason for the low efficiency of the DSSC based on WS-11.

Conclusions

We have presented a comparative study of the ground-state and excited-state properties of three D-A-π-A dyes (WS-2, WS-6, and WS-11), which were calculated using DFT/TDDFT methods. The coplanarity of the A-π-A segment and noncoplanarity of the indoline donor part of the molecule were confirmed by checking the calculated geometric parameters (bond lengths and dihedral angles). Theoretical analysis of the PDOS, total static first hyperpolarizability, frontier molecular orbitals, and excited-state charge transfer indicates that inserting an alkyl chain near the acceptor unit without damaging the coplanarity of the A-π-A segment of the sensitizer (as done in WS-6) is a feasible method of improving DSSC efficiency. The calculated absorption spectra agreed well with the corresponding experimental results. When attempting to reduce dye aggregation and improve the efficiency of the DSSC, inserting an additional electron-withdrawing substituent group that is modified by a long alkyl chain near the donor unit does not appear to be a wise choice, as it decreases the coplanarity of the bridge unit and leads to less electron delocalization and an unfavorable charge-transfer process, although the resulting molecule does show broad and intense spectral responses sometimes. We hope that our results may prove useful to synthetic chemists who are trying to find improved sensitizer molecules that could be used in highly efficient DSSCs.

Acknowledgments This work was supported by the National Natural Science Foundation of China (grant nos. 10604012 and 10974023), the Program for Liaoning Excellent Talents in University (grant no. LJQ2012002), and Program for New Century Excellent Talents in University (Grant No. NCET-12-0077).

References

1. Kuang D, Uchida S, Humphry-Baker R, Zakeeruddin SM, Gratzel M (2008) Angew Chem Int Edit 47:1923–1927
2. Mishra A, Fischer MKR, Bauerle P (2009) Angew Chem Int Edit 48: 2474–2499
3. Hwang S, Lee JH, Park C, Lee H, Kim C, Park C, Lee MH, Lee W, Park J, Kim K, Park NG, Kim C (2007) Chem Commun 4887–4889
4. Chen CY, Wang MK, Li JY, Pootrakulchote N, Alibabaei L, Ngoc-le CH, Decoppet JD, Tsai JH, Gratzel C, Wu CG, Zakeeruddin SM, Gratzel M (2009) ACS Nano 3:3103–3109
5. Gao FF, Wang Y, Shi D, Zhang J, Wang MK, Jing XY, Humphry-Baker R, Wang P, Zakeeruddin SM, Gratzel M (2008) J Am Chem Soc 130:10720–10728
6. Nazeeruddin MK, Humphry-Baker R, Liska P, Gratzel M (2003) J Phys Chem B 107:8981–8987
7. Wiberg J, Marinado T, Hagberg DP, Sun LC, Hagfeldt A, Albinsson B (2009) J Phys Chem C 113:3881–3886
8. Marinado T, Nonomura K, Nissfolk J, Karlsson MK, Hagberg DP, Sun LC, Mori S, Hagfeldt A (2010) Langmuir 26:2592–2598
9. Cao YM, Bai Y, Yu QJ, Cheng YM, Liu S, Shi D, Gao FF, Wang P (2009) J Phys Chem C 113:6290–6297
10. De Angelis F, Fantacci S, Selloni A, Nazeeruddin MK, Gratzel M (2007) J Am Chem Soc 129:14156–14157
11. Imahori H, Matsubara Y, Iijima H, Umeyama T, Matano Y, Ito S, Niemi M, Tkachenko NV, Lemmetyinen H (2010) J Phys Chem C 114:10656–10665
12. Hsieh CP, Lu HP, Chiu CL, Lee CW, Chuang SH, Mai CL, Yen WN, Hsu SJ, Diau EWG, Yeh CY (2010) J Mater Chem 20:1127–1134
13. Nazeeruddin MK, De Angelis F, Fantacci S, Selloni A, Viscardi G, Liska P, Ito S, Takeru B, Gratzel M (2005) J Am Chem Soc 127: 16835–16847

14. Nazeeruddin MK, Bessho T, Cevey L, Ito S, Klein C, De Angelis F, Fantacci S, Comte P, Liska P, Imai H, Graetzel M (2007) J Photoch Photobio A 185:331–337
15. Yella A, Lee HW, Tsao HN, Yi CY, Chandiran AK, Nazeeruddin MK, Diau EWG, Yeh CY, Zakeeruddin SM, Gratzel M (2011) Science 334:629–634
16. Yum JH, Hagberg DP, Moon SJ, Karlsson KM, Marinado T, Sun LC, Hagfeldt A, Nazeeruddin MK, Gratzel M (2009) Angew Chem Int Edit 48:1576–1580
17. Zhang GL, Bai Y, Li RZ, Shi D, Wenger S, Zakeeruddin SM, Gratzel M, Wang P (2009) Energ Environ Sci 2:92–95
18. Wang MK, Xu MF, Shi D, Li RZ, Gao FF, Zhang GL, Yi ZH, Humphry-Baker R, Wang P, Zakeeruddin SM, Gratzel M (2008) Adv Mater 20:4460–4463
19. Li RZ, Lv XJ, Shi D, Zhou DF, Cheng YM, Zhang GL, Wang P (2009) J Phys Chem C 113:7469–7479
20. Xu MF, Li RZ, Pootrakulchote N, Shi D, Guo J, Yi ZH, Zakeeruddin SM, Gratzel M, Wang P (2008) J Phys Chem C 112:19770–19776
21. Li G, Jiang KJ, Li YF, Li SL, Yang LM (2008) J Phys Chem C 112: 11591–11599
22. Haid S, Marszalek M, Mishra A, Wielopolski M, Teuscher J, Moser JE, Humphry-Baker R, Zakeeruddin SM, Gratzel M, Bauerle P (2012) Adv Funct Mater 22:1291–1302
23. Hagberg DP, Marinado T, Karlsson KM, Nonomura K, Qin P, Boschloo G, Brinck T, Hagfeldt A, Sun LC (2007) J Org Chem 72: 9550–9556
24. Zhang GL, Bala H, Cheng YM, Shi D, Lv XJ, Yu QJ, Wang P (2009) Chem Commun 2198–2200
25. Lu HP, Tsai CY, Yen WN, Hsieh CP, Lee CW, Yeh CY, Diau EWG (2009) J Phys Chem C 113:20990–20997
26. Sirohi R, Kim DH, Yu SC, Lee SH (2012) Dyes Pigments 92:1132–1137
27. Nazeeruddin MK, Pechy P, Renouard T, Zakeeruddin SM, Humphry-Baker R, Comte P, Liska P, Cevey L, Costa E, Shklover V, Spiccia L, Deacon GB, Bignozzi CA, Gratzel M (2001) J Am Chem Soc 123: 1613–1624
28. Kay A, Gratzel M (1993) J Phys Chem 97:6272–6277
29. Wang P, Zakeeruddin SM, Comte P, Charvet R, Humphry-Baker R, Gratzel M (2003) J Phys Chem B 107:14336–14341
30. Hara K, Dan-Oh Y, Kasada C, Ohga Y, Shinpo A, Suga S, Sayama K, Arakawa H (2004) Langmuir 20:4205–4210
31. Wu YZ, Zhu WH (2013) Chem Soc Rev 42:2039–2058
32. Zhu WH, Wu YZ, Wang ST, Li WQ, Li X, Chen JA, Wang ZS, Tian H (2011) Adv Funct Mater 21:756–763
33. Wu YZ, Zhang X, Li WQ, Wang ZS, Tian H, Zhu WH (2012) Adv Energy Mater 2:149–156
34. Velusamy M, Thomas KRJ, Lin JT, Hsu YC, Ho KC (2005) Org Lett 7:1899–1902
35. Hou JH, Chen HY, Zhang SQ, Li G, Yang Y (2008) J Am Chem Soc 130:16144–16145
36. Kohn W, Sham LJ (1965) Phys Rev 140:1133–1138
37. Yanai T, Tew DP, Handy NC (2004) Chem Phys Lett 393:51–57
38. Becke AD (1993) J Chem Phys 98:5648–5652
39. Lee CT, Yang WT, Parr RG (1988) Phys Rev B 37:785–789
40. Becke AD (1988) Phys Rev A 38:3098–3100
41. Binning RC, Curtiss LA (1990) J Comput Chem 11:1206–1216
42. Wachters AJH (1970) J Chem Phys 52:1033–1036
43. Hay PJ (1977) J Chem Phys 66:4377–4384
44. Krishnan R, Binkley JS, Seeger R, Pople JA (1980) J Chem Phys 72: 650–654
45. Mclean AD, Chandler GS (1980) J Chem Phys 72:5639–5648
46. Mcgrath MP, Radom L (1991) J Chem Phys 94:511–516
47. Balanay MP, Kim DH (2011) Curr Appl Phys 11:109–116
48. Liu CG, Guan W, Song P, Yan LK, Su ZM (2009) Inorg Chem 48: 6548–6554
49. Cohen HD, Roothaan CCJ (1965) J Chem Phys 43:S034–S039
50. Tsunekawa T, Yamaguchi K (1992) J Phys Chem 96:10268–10275
51. Champagne B, Jacquemin D, Andre JM, Kirtman B (1997) J Phys Chem A 101:3158–3165
52. Kleinman DA (1962) Phys Rev 126:1977–1979
53. Stratmann RE, Scuseria GE, Frisch MJ (1998) J Chem Phys 109: 8218–8224
54. Tomasi J, Mennucci B, Cammi R (2005) Chem Rev 105:2999–3093
55. Cances E, Mennucci B, Tomasi J (1997) J Chem Phys 107:3032–3041
56. Mennucci B, Tomasi J (1997) J Chem Phys 106:5151–5158
57. Tomasi J, Mennucci B, Cances E (1999) J Mol Struc–Theochem 464: 211–226
58. O'Boyle NM, Tenderholt AL, Langner KM (2008) J Comput Chem 29:839–845
59. Sun MT, Liu LW, Ding Y, Xu HX (2007) J Chem Phys 127:084706
60. Sun MT, Kjellberg P, Beenken WJD, Pullerits T (2006) Chem Phys 327:474–484
61. Sun MT, Liu SS, Chen MD, Xu HX (2009) J Raman Spectrosc 40: 137–143
62. Frisch MJTT, GW, Schlegel HB, Scuseria GE, Robb MA, Cheeseman JR, Scalmani G, Barone V, Mennucci B, Petersson GA, Nakatsuji H, Caricato M, Li X, Hratchian HP, Izmaylov AF, Bloino J, Zheng G, Sonnenberg JL, Hada M, Ehara M, Toyota K, Fukuda R, Hasegawa J, Ishida M, Nakajima T, Honda Y, Kitao O, Nakai H, Vreven T, Montgomery JA Jr, Peralta JE, Ogliaro F, Bearpark M, Heyd JJ, Brothers E, Kudin KN, Staroverov VN, Kobayashi R, Normand J, Raghavachari K, Rendell A, Burant JC, Iyengar SS, Tomasi J, Cossi M, Rega N, Millam JM, Klene M, Knox JE, Cross JB, Bakken V, Adamo C, Jaramillo J, Gomperts R, Stratmann RE, Yazyev O, Austin AJ, Cammi R, Pomelli C, Ochterski JW, Martin RL, Morokuma K, Zakrzewski VG, Voth GA, Salvador P, Dannenberg JJ, Dapprich S, Daniels AD, Farkas O, Foresman JB, Ortiz JV, Cioslowski J, Fox DJ (2009) Gaussian 09. Gaussian Inc., Wallingford
63. Choi H, Baik C, Kang SO, Ko J, Kang MS, Nazeeruddin MK, Gratzel M (2008) Angew Chem Int Edit 47:327–330
64. Ning ZJ, Zhang Q, Wu WJ, Pei HC, Liu B, Tian H (2008) J Org Chem 73:3791–3797
65. Peach MJG, Tellgrent EI, Salek P, Helgaker T, Tozer DJ (2007) J Phys Chem A 111:11930–11935
66. Jacquemin D, Perpete EA, Scalmani G, Frisch MJ, Kobayashi R, Adamo C (2007) J Chem Phys 126:144105
67. Limacher PA, Mikkelsen KV, Luthi HP (2009) J Chem Phys 130:194114
68. Wonneberger H, Pschirer N, Bruder I, Schoneboom J, Ma CQ, Erk P, Li C, Bauerle P, Mullen K (2011) Chem–Asian J 6:1744–1747
69. Cahen D, Hodes G, Gratzel M, Guillemoles JF, Riess I (2000) J Phys Chem B 104:2053–2059
70. Laurent AD, Jacquemin D (2013) Int J Quantum Chem 113:2019–2039
71. Manzhos S (2013) MRS Commun 3:37–39
72. Wu YZ, Marszalek M, Zakeeruddin SM, Zhang Q, Tian H, Gratzel M, Zhu WH (2012) Energ Environ Sci 5:8261–8272
73. Ding WL, Wang DM, Geng ZY, Zhao XL, Xu WB (2013) Dyes Pigments 98:125–135
74. Clark AE, Qin CY, Li ADQ (2007) J Am Chem Soc 129:7586–7595
75. Pastore M, De Angelis F (2010) ACS Nano 4:556–562
76. Koumura N, Wang ZS, Mori S, Miyashita M, Suzuki E, Hara K (2006) J Am Chem Soc 128:14256–14257
77. Li YZ, Pullerits T, Zhao MY, Sun MT (2011) J Phys Chem C 115: 21865–21873
78. Li YZ, Shi Y, Chen MD, Li YQ, Su RZ, Zhao MY, Ma FC (2012) J Mol Model 18:4141–4149
79. Sun MT (2006) J Chem Phys 124:054903
80. Sun MT, Chen JN, Xu HX (2008) J Chem Phys 128:064106
81. Song P, Li YZ, Ma FC, Pullerits T, Sun MT (2013) J Phys Chem 117: 15879–15889